Published online 31 July 2012 *Nucleic Acids Research, 2012, Vol. 40, No. 19* ***9429–9440***
doi:10.1093/nar/gks716

The histone demethylase PHF8 is essential for cytoskeleton dynamics

Elena Asensio-Juan[1], Carme Gallego[2] and Marian A. Martínez-Balbás[1,*]

[1]Department of Molecular Genomics and [2]Department of Cell Biology, Instituto de Biología Molecular de Barcelona (IBMB), Spanish Research Council (CSIC), Barcelona Science Park (PCB), Barcelona 08028, Spain

Received February 29, 2012; Revised June 16, 2012; Accepted July 4, 2012

ABSTRACT

PHF8 is a histone demethylase associated with X-linked mental retardation. It has been described as a transcriptional co-activator involved in cell cycle progression, but its physiological role is still poorly understood. Here we show that PHF8 controls the expression of genes involved in cell adhesion and cytoskeleton organization such as RhoA, Rac1 and GSK3β. A lack of PHF8 not only results in a cell cycle delay but also in a disorganized actin cytoskeleton and impaired cell adhesion. Our data demonstrate that PHF8 directly regulates the expression of these genes by demethylating H4K20me1 at promoters. Moreover, c-Myc transcription factor cooperates with PHF8 to regulate the analysed promoters. Further analysis in neurons shows that depletion of PHF8 results in down-regulation of cytoskeleton genes and leads to a deficient neurite outgrowth. Overall, our results suggest that the mental retardation phenotype associated with loss of function of PHF8 could be due to abnormal neuronal connections as a result of alterations in cytoskeleton function.

INTRODUCTION

X-linked mental retardation (XLMR) is a highly diverse group of cognitive disorders. The high incidence of XLMR makes this disorder an important problem in medicine (1,2). A strikingly large number of genes mutated in XLMR encode for regulators of chromatin structure (2,3). One of these is the gene that codes for PHF8, a histone demethylase (HDM) (4–6). PHF8 belongs to a family of plant homeodomain (PHD) finger-containing HDMs which in humans is formed by PHF2, PHF8 and KIAA1718. These proteins contain an N-terminal PHD and a Jumonji-C (JmjC) domain (7). Deletions and point mutations in the PHF8 JmjC domain lead to Siderius–Hamel syndrome, mild XLMR with cleft lip and/or a cleft palate (CL/P) (4,8–10).

PHF8 binds through its PHD to H3K4me3 nucleosomes at the transcription start site (TSS) regions of active promoters (11–14). Moreover, PHF8 catalytic activity removes mono- and dimethyl-lysine 9 and 27 on histone H3 and monomethyl-lysine 20 on histone H4 (11,12,14,15). All these are repressive histone modifications, suggesting that PHF8-mediated removal of these marks leads to transcriptional activation. In line with this, knockdown (KD) of PHF8 leads to down-regulation of several genes (11,12). Interestingly, some PHF8 target genes are involved in XLMR, such as JARID1C, or in neural development, such as MSX1 (11,16). Moreover, KD of the PHF8 homolog in zebrafish causes brain and craniofacial developmental anomalies (13,16) and alters neuronal differentiation of murine P19 cells (17). In addition, loss of the PHF8 homolog in *Caenorhabditis elegans* leads to an overall increase in H3K9me2 and affects body movement (11).

It has also been proposed that PHF8 affects cell cycle progression by facilitating E2F1-mediated transcriptional activation (15) and that PHF8 co-activates rRNA transcription (18,19). Although it is well established that PHF8 alters gene expression, it is still unclear how PHF8 mutations lead to XLMR. Indeed, the PHF8-regulated gene expression changes are subtle; this suggests that not only a single gene pathway is responsible for the PHF8 phenotype but also a combination of modification may underlie this condition. Our results show that PHF8 controls the expression of some key regulators of the cytoskeleton such as RhoA, Rac1 and GSK3β. Depletion of PHF8 has a striking effect on cellular cytoskeleton structure and impairs neurite elongation. These findings suggest that the XLMR phenotype associated with PHF8 mutations could be due to alterations in the cytoskeleton structure.

*To whom correspondence should be addressed. Tel: +34 93 403 49 61; Fax: +34 93 403 49 79; Email: mmbbmc@ibmb.csic.es

MATERIALS AND METHODS

Cell culture, transfections and co-immunoprecipitation assays

HeLa, HEK293T and SH-SY5Y cells were grown under standard conditions (20). CoIP experiments with transfected proteins were performed as described elsewhere (21).

Primary neuronal cultures were prepared from cerebral cortices of E17 mouse, sliced into 1-mm pieces and treated with trypsin (0.05%, for 20 min at 37°C; Invitrogen). The tissue was mechanically dissociated by passing through a flame-polished Pasteur pipette. Cells were plated at 1×10^4 cells/cm^2 on poly-D-lysine-coated (0.5 mg/ml) plates and maintained in Neurobasal basal medium (Invitrogen) supplemented with B27 (Invitrogen), penicillin/streptomycin and glutamine at 2 mM.

Plasmids

PHF8-HA was kindly provided by Dr Christoph Loenarz, Flag-N-Myc by Dr Elisa Martí and Flag-c-Myc by Dr Keiichi Nakayama. Flag-E47 has been previously described (22). mPhf8 cDNA was cloned into pCDNA3 vector and the mutant HD>AA was generated using the QuickChange II XL Site-Directed Mutagenesis kit (Stratagene). The residues H247 and D249 at the *jumonji* domain were mutated to A. Finally, it was cloned into the polycistronic vector pCIG that co-expresses green fluorescent protein (GFP).

Viral vectors were purchased from Sigma: pLKO-hPHF8#1 (GCAGGTAAATGGGAGAGGTTT), pLKO-hPHF8#2 (CGAACCGTACAGCTCATTAAA), pLKO-mPhf8-GCGGACTGTACAGCTCATTAA and pLKO-random (CAACAAGATGAAGAGCACC). Transient KD in HeLa cells was performed using the pSuper vector with a non-specific sequence (GGCTGAATGCAA GCGTGGA) or one specific to the human PHF8 sequence (GAGGAGAAGGCTGCTGACA).

Antibodies and reagents

Antibodies used were anti: PHF8 (Abcam ab36068), c-Myc (Santa Cruz Biotechnology sc-764), HA (Sigma H6908), FLAG M2 (Sigma F3165), H4K20me1 (Abcam ab9053), β-catenin (Sigma C7207) and β-tubulin (Chemicon MAB3408). Fibrillar actin was stained with phalloidin–rhodamine (Sigma P1951).

Microarray analysis

RNAs from 10^6 HeLa cells were supplied to the Microarrays Unit of the Center for Genomic Regulation (CRG, Barcelona, Spain) for quality control, quantification, reverse transcription, labelling and hybridization using an Illumina Platform with Whole Human Genome microarrays. Triplicates were analysed for each sample. Fold changes (FCs) between control and PHF8-depleted samples were calculated applying the Array File Maker 4.0 (AFM 4.0) toolbox (23). Briefly, differential expression analysis was performed on non-control probes with an empirical Bayes approach on linear models (Limma) (24), and the results were corrected for multiple testing according to the false discovery rate (25). Normalized data are available at the Gene Expression Omnibus database (http://www.ncbi.nlm.nih.gov/geo/) with the accession number GSE38175.

ChIP-Seq analysis

PHF8 ChIP-Seq data were downloaded from Gene Expression Omnibus database (GSM531964) (16) and analysed with the ChIP-Seq Tool Set (26) in order to obtain PHF8 target genes and the peak intensity.

Chromatin immunoprecipitation assays

Chromatin immunoprecipitation (ChIP) assays were performed using previously described procedures with few modifications (27). Fixation with 1% formaldehyde was stopped by the addition of 0.125 mM glycine. Cytoplasms were lysed with cell lysis buffer (20 mM Tris–HCl pH 8, 85 mM KCl, 0.5% NP40). Nuclei were isolated by centrifugation at 5000 rpm and resuspended in nuclei lysis buffer (1% sodium dodecyl sulphate (SDS), 10 mM ethylenediaminetetraacetic acid (EDTA) and 50 mM Tris pH 8). The sonication step was performed in a Bioruptor sonicator (to obtain ~500 bp fragments) and 0.1 mg of protein was diluted in IP buffer (1% Triton, 2 mM EDTA, 150 mM NaCl and 20 mM Tris pH 8) for each immunoprecipitation. The antibody–protein complex was captured using pre-blocked protein A (Millipore 16-157) and DNA purification performed using phenol/chloroform. Finally, ChIP DNA was analysed by quantitative polymerase chain reaction (qPCR). with SYBR Green (Roche) in a LightCycler 480 PCR system (Roche). For re-ChIP experiments, 0.3 mg of protein was used as starting material. After the first ChIP with anti-PHF8 antibody, protein–DNA complexes were eluted in 50 µl 10 mM Dithiothreitol (DTT) for 30 min at 37°C, diluted in IP buffer and subjected again to the ChIP procedure with anti-c-Myc antibody.

Percentage of input was calculated from specific immunoprecipitation enrichment values obtained by qPCR with respect to the total starting chromatin (that is the input material).

Immunoblotting

Immunoblotting was performed by standard procedures and visualized on an Odyssey Infrared Imager (Li-Cor).

Messenger RNA extraction and qPCR

TRIZOL reagent (Invitrogen) was used to extract messenger RNA (mRNA), following the manufacturer's instructions. Reverse transcription was then performed with a Transcription kit (Roche) following the manufacturer's procedure, and qPCR was performed with SYBR Green (Roche) in LightCycler 480 (Roche).

Indirect immunofluorescence

Cells were fixed for 20 min in 4% paraformaldehyde and permeabilized with Phosphate buffered saline–Triton 0.1%. Indirect immunofluorescence was performed as described previously (21).

Lentiviral transduction

HEK293T cells growing in a 10-cm dish were transfected with a mix of packaging, envelop and short hairpin RNA (shRNA) transfer vector DNAs (6, 5 and 7 μg, respectively). After 30 h of transfection, the medium was collected and the virus concentrated by ultracentrifugation (26 000 rpm, 2 h at 4°C). Viral particles were then added to receptor cells. After 24 h, transduced cells were selected with puromycin (HeLa: 5 μg/ml, SH-SY5Y: 0.5 μg/ml). Cortical neurons were infected when plated; viruses were removed 24 h later and neurons were cultured for another 3 days before use. Instead of selection, viruses were added to infect an 80% of the cells. Finally, the efficiency of KD constructs was assessed by qPCR and immunoblot. Plasmids were purchased from Sigma.

Neurite length quantification

Pictures were taken of 10 randomly selected fields of phalloidin–rhodamine and 4′,6-diamidino-2-phenylindole (DAPI) stained SH-SY5Y and cortical cells. The total length of neurites was calculated by using ImageJ software, and related to total number of cells (quantified by DAPI).

Statistical analysis

Quantitative data were expressed as mean and standard deviation (SD) of at least three biologically independent experiments. The significance of differences between groups was assessed using Student's *t*-test ($*P < 0.05$; $**P < 0.01$; $***P < 0.001$).

RESULTS

PHF8 regulates cytoskeleton and cell adhesion gene expression

To understand how PHF8 might contribute to XLMR, we set out to identify genes whose regulation was compromised in the absence of PHF8. To this end, we performed a microarray expression experiment with control and PHF8-depleted HeLa cells transiently transfected with a random shRNA or with a PHF8 shRNA, which efficiently decreases PHF8 levels (Figure 1A). The RNA was extracted, labelled and hybridized to Illumina gene expression arrays. Then, we selected genes showing FCs ≥ 1.2 and ≤ -1.2 with an adjusted *P*-value ≤ 0.05 between the two conditions. We identified 259 (55%) up-regulated and 211 (45%) down-regulated genes in PHF8-depleted cells (Figure 1B) relative to control cells. Microarray results were verified by using qPCR to check 12 genes with different FC and *P*-values (Figure 1C and Supplementary Figure S1A). The mRNA levels of PHF8 homologs, KIAA1718 and PHF2, also were checked to confirm that the shRNAs did not affect the expression of these genes (Supplementary Figure S1B). In order to confirm the specificity of the used shRNA, we performed two experiments: (i) first, we knocked down PHF8 with a second independent PHF8 shRNA (Supplementary Figure S1C) and checked by qPCR the expression of the same set of genes. The results in Supplementary Figure S1D showed that the expression of the analysed genes was also affected; (ii) second, over-expression of murine Phf8 (mPhf8) protein (Supplementary Figure S1E), resistant to the human PHF8 shRNA, restored the expression of most of the analysed genes (Figure 1C, green boxes).

To further characterize the transcriptional differences between control and PHF8-depleted cells, we assessed the molecular and cellular functions over-represented in the identified PHF8-dependent genes using Ingenuity Pathway Analysis (Ingenuity Systems). We found that the groups with the most significant enrichment of down-regulated genes or the total set of PHF8-regulated genes were associated with cellular morphology and dynamics (Figure 1D, upper panel and Supplementary Figure S1F). In particular, several genes involved in the Rho signalling pathway (RhoA, Rac1, mDia1) and in cell–cell contact (α-catenin) were severely affected by PHF8 depletion. These functional categories were not over-represented in the up-regulated genes (Figure 1D lower panel). These data suggest that the ability of PHF8 to regulate genes associated with cellular morphology and dynamics might be linked to the transcriptional co-activator function described for PHF8 (11,12). Further, genes involved in cell growth and proliferation are also significantly enriched (as previously shown) (15). In line with this, cell growth defects were observed in PHF8-depleted cells (Supplementary Figure S2). Comparison of our results with genome-wide localization of PHF8-binding sites along the genome performed in HeLa cells (16) indicated that 51% of the genes differentially expressed in the microarray (deregulated) were PHF8 direct targets; from these, 62% were down-regulated and 38% up-regulated (Figure 1E and Supplementary Figure S3A). In contrast, only 15% of non-deregulated genes were bound by PHF8 (Figure 1E). On the other hand, 3% of PHF8 target genes identified by ChIP-Seq (16) were differentially expressed upon PHF8 KD, in concordance with previous results showing that few PHF8 target genes were transcriptionally affected by PHF8 depletion (11). In agreement with our previous data, analysis of the molecular and cellular functions over-represented in the identified PHF8-direct target and deregulated genes indicated that the cellular morphology and dynamics groups were again significantly enriched (Supplementary Figure S1G). In order to understand why few PHF8 target genes were differentially expressed upon PHF8 depletion, we compared PHF8-binding intensity (detected by ChIP-Seq) between different sets of genes. The results in Supplementary Figure S3B and C showed that there were no significant differences in PHF8-binding intensity between deregulated and non-deregulated genes or between up- and down-regulated genes in the microarray.

PHF8 reduction leads to cytoskeleton disorganization and cell adhesion alterations

Based on the aforementioned results and because the PHF8-associated phenotype (XLMR with or without CL/P) is related to cell adhesion and cytoskeleton

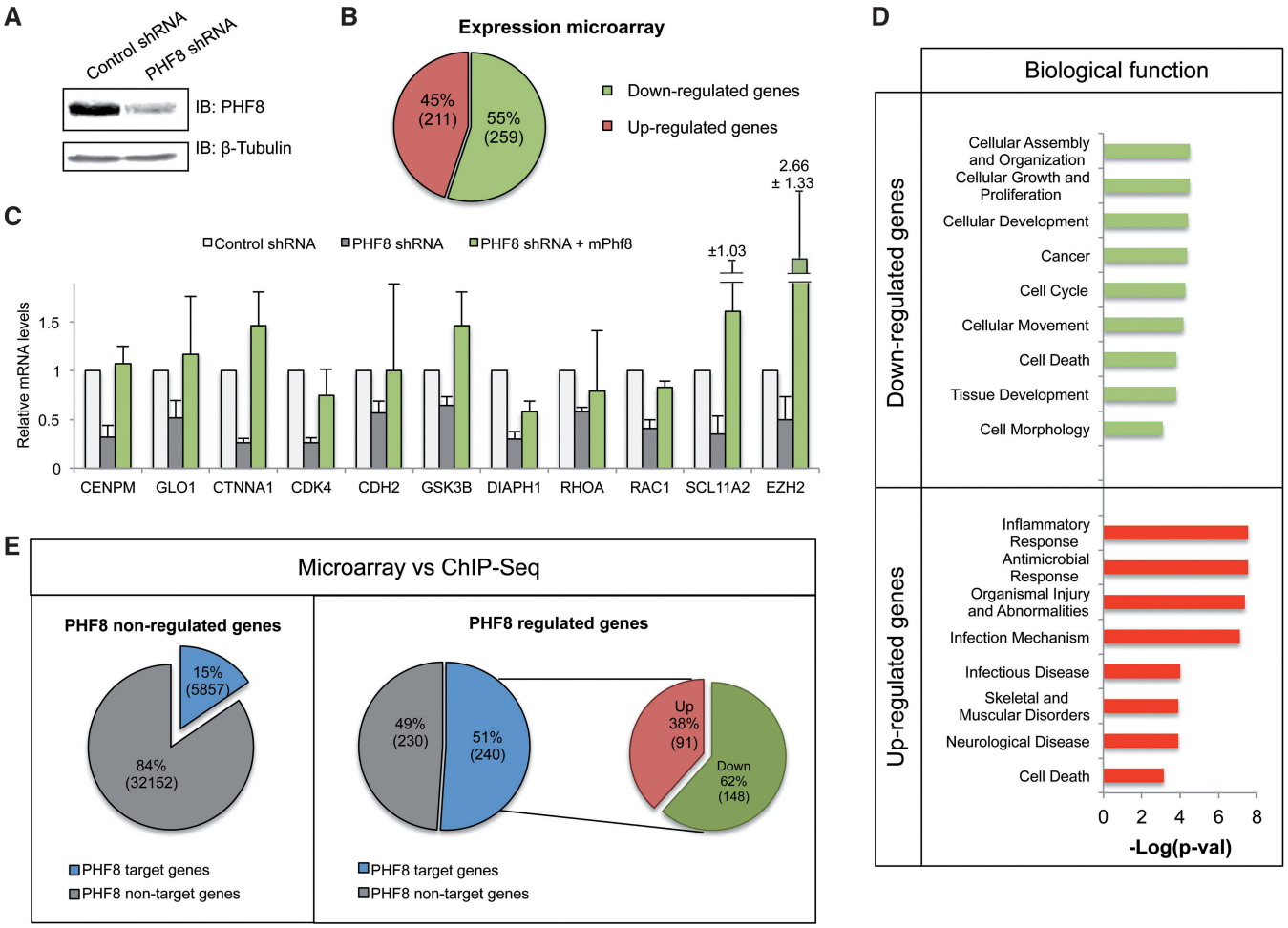

Figure 1. PHF8 regulates cytoskeleton and cell adhesion gene expression. (**A**) PHF8 was depleted from HeLa cells with a specific shRNA. A random shRNA was used as a control. Total cell lysates were immunoblotted with anti-PHF8 and anti-β tubulin as a loading control. (**B**) Diagram showing the number and percentage of up- and down-regulated genes in the microarray expression analysis. (**C**) Some selected genes in the microarray were validated by qPCR. The data were normalized by 18S mRNA levels. Error bars indicate SD (**D**) The genes in the microarray were analysed with Ingenuity Pathway Analysis. The chart shows the over-represented biological functions for down-regulated (upper panel) and up-regulated genes (lower panel). (**E**) Diagrams showing the number and percentage of differentially expressed genes in the microarray (PHF8 regulated genes) that are PHF8 direct targets in ChIP-Seq experiments (right panel). The percentage of PHF8 non-regulated genes that are bound by PHF8 is shown on the left panel.

organization (1,28,29), we sought to investigate whether PHF8 could regulate these processes. To this end, we established two PHF8 KD lines of HeLa cells by transduction with lentiviral particles containing PHF8 shRNA (PHF8 KD) or a random shRNA sequence (Control KD). Immunoblot analysis confirmed that PHF8 shRNAs efficiently decrease the PHF8 protein, although to different degrees (line#1 had lower levels than #2) (Figure 2A) without affecting the expression levels of the PHF8 homologs, KIAA1718 and PHF2 (Supplementary Figure S4A and B). Then, we analysed the effects of PHF8 depletion on cytoskeleton structure and cell adhesion. To this end, Control and PHF8 KD cells were stained with phalloidin–rhodamine and β-catenin antibody. The results in Figure 2B showed a strong effect of PHF8 depletion on cellular structure. Phalloidin staining revealed that control cells are polygonal, and they are strongly bound together (Figure 2B and C-i, ii). The cytoskeleton is disorganized in PHF8 KD cells and they are more rounded and less flat than Control KD cells (Figure 2B, and C-iii, iv). In addition, PHF8 KD cells have more filopodia than control cells (Figure 2B and 2C-v, vi). Moreover, β-catenin staining evidences that cell–cell contact is partially lost (Figure 2B). In order to confirm that the observed phenotype is due to PHF8 activity, we used a PHF8 mutant that lacks HDM activity (PHF8 HD>AA, see 'Materials and Methods' section) (5). Over-expression of this inactive protein (Supplementary Figure S1E) resulted in an increased number of the rounded cells (from 19% in GFP over-expressing cells to 62.6% in PHF8 HD>AA) (Figure 2D).

As many of the identified gene products are involved in focal adhesion, we analysed the ability of PHF8-depleted cells to attach to the substrate. To that end, the same numbers of Control KD and PHF8 KD#1 (from now on PHF8 KD) cells were plated and the number of attached cells was quantified at different time points

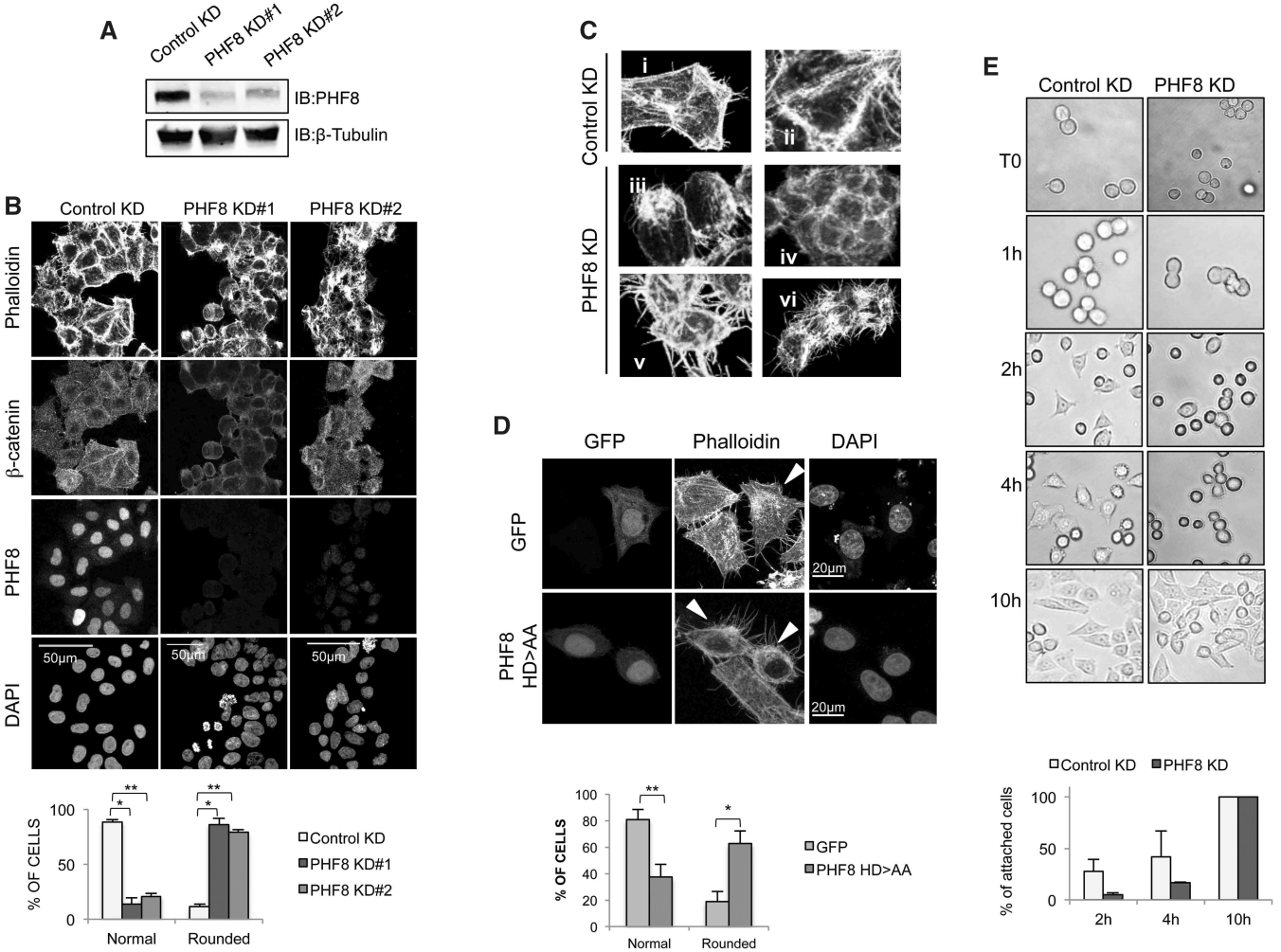

Figure 2. PHF8 KD cells have disorganized actin cytoskeleton and adhesion defects. (**A**) Immunoblot from Control KD, PHF8 KD#1 and PHF8 KD#2 cell extracts using the indicated antibodies. (**B**) Control and PHF8 KD cells were stained with phalloidin–rhodamine and anti-β-catenin to visualize the cytoskeleton structure and cell–cell contacts. The number of round cells in each sample was quantified by direct counting in different experiments. Data show mean of $n = 500$ cells. Error bars indicate SD $*P < 0.05$; $**P < 0.01$. The percentage of total cells counted is represented. (**C**) Details of the cytoskeleton structure of Control and PHF8 KD cells. (**D**) HeLa cells were transfected with pCIG (GFP) or pCIG-PHF8 HD>AA (PHF8 HD>AA). Then, cells were stained with phalloidin–rhodamine and DAPI. Transfected cells (GFP positive) were analysed. The number of green and round cells was quantified by direct counting. Data show mean of $n = 100$ cells. Error bars indicate SD $*P < 0.05$; $**P < 0.01$. (**E**) Pictures of Control and PHF8 KD cells were taken at different times after seeding. Cells were fixed and stained with crystal violet at different times after seeding. The intensity of the staining was quantified with ImageJ software. Results are the mean of three independent experiments. Data show mean of $n = 700$ cells. Error bars indicate SD.

(by quantifying crystal violet-stained cells after fixing). Pictures taken at different times showing that PHF8 KD cells take longer to attach to the substrate (Figure 2E). Quantification indicated that 2 h after plating, Control KD cells began to attach (27.8% cells attached), while PHF8 KD cells were less able to bind (5% cells attached). These differences were maintained for 4 h (41.9% of control cells had become attached while only 16.4% of PHF8 KD cells had bound to the plate) (Figure 2E). After 10 h, almost all cells were attached to the plate in both cases. Taken together these data suggest that PHF8 depletion leads to a strong alteration in cell structure and dynamics. Moreover, they indicate that PHF8 HDM activity is required for the proper cell structure organization.

PHF8 directly regulates cytoskeleton-related genes

At this point, our data suggested that PHF8 played an essential role in regulating cytoskeleton gene expression. To understand how PHF8 might contribute to this transcriptional control, we tested whether these genes are direct targets of PHF8. To this end, we performed ChIP experiments in Control and PHF8 KD cells and analysed the promoters of a subset of genes by qPCR. We selected some genes that were down-regulated in the microarray experiment and that are essential for defining cell structure and dynamics: RhoA, GSK3β and α-catenin. The results, illustrated in Figure 3A, demonstrated that PHF8 is bound to the TSS region of the analysed promoters but not to control promoters: OLIG2 (an inactive gene) and

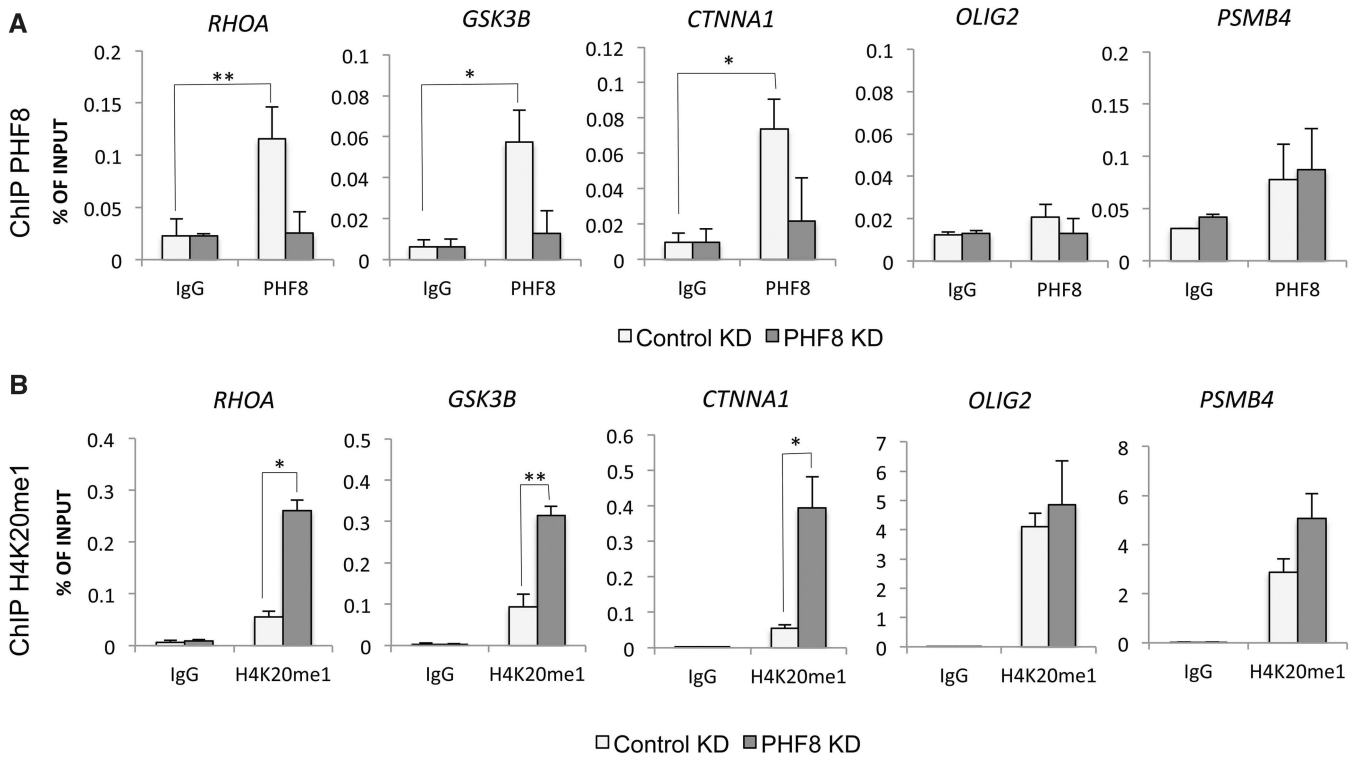

Figure 3. PHF8 demethylates H4K20me1 at promoters. (**A**) ChIPs of PHF8 in Control and PHF8 KD cells analysed by qPCR, at the TSS of the indicated genes. (**B**) ChIP of H4K20me1 in Control and PHF8 KD cells. Results are the mean of three independent experiments. Error bars indicate SD $*P < 0.05$; $**P < 0.01$.

PSMB4 (an active gene). As PHF8 is a HDM for H4K20me1, we compared the levels of this histone modification at the analysed promoters in Control and PHF8 KD cells. The results shown in Figure 3B indicate that methylation increases at the promoter level after PHF8 depletion. These data strongly suggest that PHF8 directly regulates the expression of the analysed genes.

PHF8 cooperates with Myc transcription factor to regulate transcription

Next, we sought to investigate how PHF8 is targeted to cytoskeleton gene promoters. To do that, we analysed the promoter sequences of genes whose expression is affected by the depletion of PHF8 identified in the microarray experiment using the PEAKS tool (30). We checked 400 bp upstream and 200 downstream of the TSS. Binding sites (with a *P*-value lower than 1 e-18) for E2F1, Sp1, Foxo1, TCF and Myc-Max among others were identified (Supplementary Figure S5A). As c-Myc transcription factor has recently been reported to be a key regulator of RhoA expression (31), and PHF8 cooperates with c-Myc in transcriptional activation (12), we decided to investigate whether Myc could contribute to PHF8-mediated transcriptional regulation of the analysed genes. To address this question, we first decreased transiently the c-Myc protein levels of HeLa cells by transduction with lentiviral particles containing c-Myc shRNA (c-Myc KD). Immunoblot analysis confirmed that c-Myc shRNA decreases c-Myc protein while PHF8 levels were not affected (Figure 4A). Then, we determined by qPCR the mRNA levels of RhoA, GSK3β and α-catenin in cells transduced with control and c-Myc shRNAs. The results shown in Figure 4B indicate that c-Myc is essential for an efficient transcription of the analysed PHF8-regulated genes. Then, we sought to determine whether c-Myc binds the analysed gene promoters. Our ChIP results in Figure 4C demonstrate that c-Myc factor efficiently binds RhoA, GSK3β and α-catenin promoters in Control cells, but not in c-Myc KD cells. The results described above demonstrate that c-Myc and PHF8 regulate and bind to the same set of genes, thus we tested whether c-Myc and PHF8 bind simultaneously to the same nucleosomes. To address this question, we performed re-ChIP experiments, immunoprecipitating sequentially PHF8 and c-Myc factors from HeLa cells. Figure 4D shows a significant enrichment of PHF8 and c-Myc factors on RhoA and α-catenin promoters after both immunoprecipitations, suggesting that these proteins bind simultaneously to some promoters.

Given this, we wondered whether c-Myc is required for PHF8 recruitment to RhoA, α-catenin and GSK3β promoters. To address this question, we first compared the binding of c-Myc in Control, PHF8 KD and c-Myc KD cells using ChIP assays. Our results showed that c-Myc binds to the promoters in Control and PHF8 KD cell lines (Figure 4E). Then, we checked the binding of PHF8 in Control, c-Myc KD and PHF8 KD cells. Figure 4F shows that PHF8 binding to promoters observed in Control cells was significantly reduced in c-Myc KD cells, suggesting that c-Myc is required for

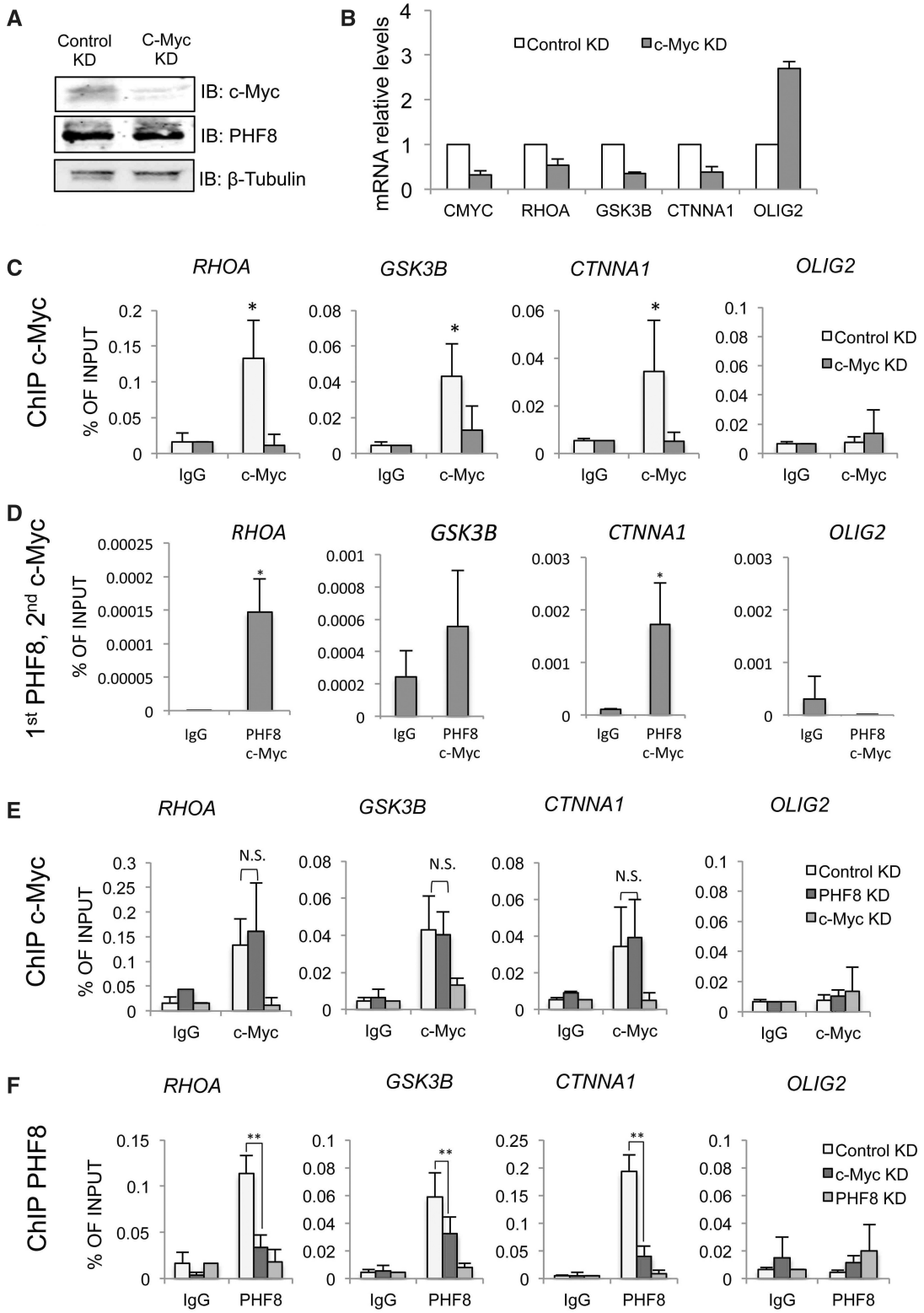

Figure 4. PHF8 and c-Myc cooperate to regulate the expression of the same genes. (**A**) Immunoblot of c-Myc, PHF8 and β-tubulin in Control and c-Myc KD HeLa cells. (**B**) mRNA levels of several PHF8-dependent cytoskeleton and cell adhesion genes in c-Myc KD cells quantified by qPCR. The data were normalized by 18S mRNA levels. Results are the mean of two independent experiments. Error bars indicate SD (**C**) ChIPs of c-Myc in Control and c-Myc KD cells analysed by qPCR at the indicated promoters. (**D**) Re-ChIP experiments in HeLa WT cells. After the first ChIP with anti-PHF8 antibody, protein–DNA complexes were eluted and immunoprecipitated with anti-c-Myc antibody. (**E**) ChIPs of c-Myc analysed by qPCR at the promoter of several genes in Control KD, PHF8 KD and c-Myc KD cell lines. (**F**) ChIPs of PHF8 in Control KD, c-Myc KD and PHF8 KD cell lines. Results are the mean of three independent experiments. Error bars indicate SD $*P < 0.05$; $**P < 0.01$. (N.S.) Non-significant.

PHF8 binding to the analysed promoters. Given that PHF8 binds to H3K4me3 nucleosomes through its PHD domain (11,12), we tested whether the lower binding in c-Myc KD cells was due to a decrease in H3K4me3 level after c-Myc depletion. ChIP experiments in Control and c-Myc KD cells showed no differences in H3K4me3 level between the two cell lines (Supplementary Figure S5B). These data are in concordance with previous results showing that MLL (the enzyme that trimethylates H3K4) recruitment to promoters is previous to Myc binding (32). Taken together, these results indicate that c-Myc contributes to PHF8 targeting to some cytoskeleton gene promoters but not vice versa. Finally, we checked whether PHF8 and Myc proteins are able to interact. Co-immunoprecipitation (Co-IP) experiments with over-expressed proteins indicated that PHF8 interacts with both c-Myc and N-Myc (the neural Myc form), but not with another bHLH factor (E47) (Supplementary Figure S5C). However, we did not detect binding of the endogenous proteins under the studied conditions in agreement with previous data (12).

All together our results indicate that PHF8 forms part of the Myc-mediated transcriptional complex that regulates the activity of some genes involved in cell structure and dynamics.

Down-regulation of PHF8 leads to alterations in neurite outgrowth

The elongation and guidance of neurites as well as the formation of dendritic spines require the integration of cell signalling and gene transcription events (29,33). Alterations of cytoskeleton molecules in neuronal cells affect the structure and function of dendritic spines, synapses and axon elongation. In line with that, changes in the activity of the small GTPases RhoA and Rac1 have been associated with mental retardation disorders (29,34,35).

Due to the essential role of cell adhesion and cytoskeleton molecules in the function of neuronal circuits, we analysed whether low levels of PHF8 could affect neurite outgrowth. To test this hypothesis, the levels of PHF8 were transiently reduced in the neuroblastoma cell line SH-SY5Y and the presence of neurites was monitored by phalloidin staining. Supplementary Figure S6A shows that transfected cells lose neurites and the actin cytoskeleton collapses. In order to confirm these results, SH-SY5Y cell line was infected with lentivirus expressing two different shRNAs against PHF8 or the control shRNA. In agreement with our previous results, cells with low levels of PHF8 were more rounded and less flat than Control KD cells, they formed foci and replicated very slowly (Figure 5A). The PHF8 KD#1 cells were not able to proliferate and so all the experiments were performed in PHF8 KD #2 cell line. We first checked the expression of the analysed genes (RhoA, GSK3β and α-catenin) and other down-regulated genes in the microarray (Figure 1) required for neuritogenesis (Diaph1 and Rac1). The expression of these genes was also PHF8-dependent in SH-SY5Y cells (Figure 5B). Moreover, Gene Ontology analysis of PHF8-direct target genes identified by genome-wide analysis in the SH-SY5Y cell line (11) showed that the most enriched categories are ones related to cytoskeleton dynamics (Supplementary Figure S6B).

Based on these results, we next sought to investigate the ability of PHF8-depleted cells to form neurites using phalloidin staining. The results showed that the number and length of neurites are markedly lower in cells with low levels of PHF8 (Figure 5C). Finally, we investigated whether PHF8-depleted cells elongated neurites upon neuronal differentiation induced by retinoic acid treatment. The results demonstrated that PHF8-depleted cells have a limited ability to generate and to extend neurites (Figure 5D). Moreover, over-expression of the catalytically inactive mutant PHF8 HD>AA altered the structure of transfected cells (69%) when compared with GFP-transfected cells (39%) (Figure 5E). This result suggests that PHF8 HDM activity is required for neuritogenesis.

As PHF8 is highly expressed in cerebral and cerebellar cortex (10), we sough to confirm our results in primary neuronal cultures derived from the mouse cerebral cortex (see 'Materials and Methods' section). In order to reduce PHF8 levels, cortical neurons were infected with lentivirus expressing shRNA against mPhf8 or the control shRNA, and the length and morphology of neurites were monitored by phalloidin staining at 4DIV (Days in vitro) (Figure 6). mPhf8 down-regulation was confirmed by checking the mRNA levels by qPCR (Figure 6A). Neurons with low levels of mPhf8 showed a general alteration of the cellular morphology (Figure 6B-i and iv). In particular, the number of neurites per cell was clearly reduced when compared with neurons expressing the control shRNA, going from 4–5 in control to 2–3 in mPhf8 KD neurons (Figure 6B ii and v; quantified in Figure 6C). Interestingly, in mPhf8 KD cultures, a high number of cells presented only a single or none neurites (Figure 6B v and Figure 6C). In addition, the neurite length was also reduced (Figure 6B iii and vi; quantified in Figure 6D). A dramatic effect of mPhf8 depletion on neurite structure was also observed at the growth cones: they were not well defined and presented filopodia in different directions, resulting in wider neurites than in control neurons (arrows in Figure 6B v-vi). Furthermore, the number and length of secondary neurites were also reduced in mPhf8 KD cells (Figure 6B). As a consequence of both, a reduced length and number of neurites, the connexions between neighbouring neurons were also affected in KD PHF8 compared with control neurons. In accordance with these results, over-expression of PHF8 HD>AA did not allow the growth and branching of neurites (Figure 6E).

Overall, these results suggest that PHF8 is essential for normal growth and stabilization of neurites during neuritogenesis. Accordingly, low levels or complete loss of function of PHF8 could lead to impaired neuronal connections.

DISCUSSION

XLMR is a complex set of disorders in which a large number of genes are involved; this makes it very difficult

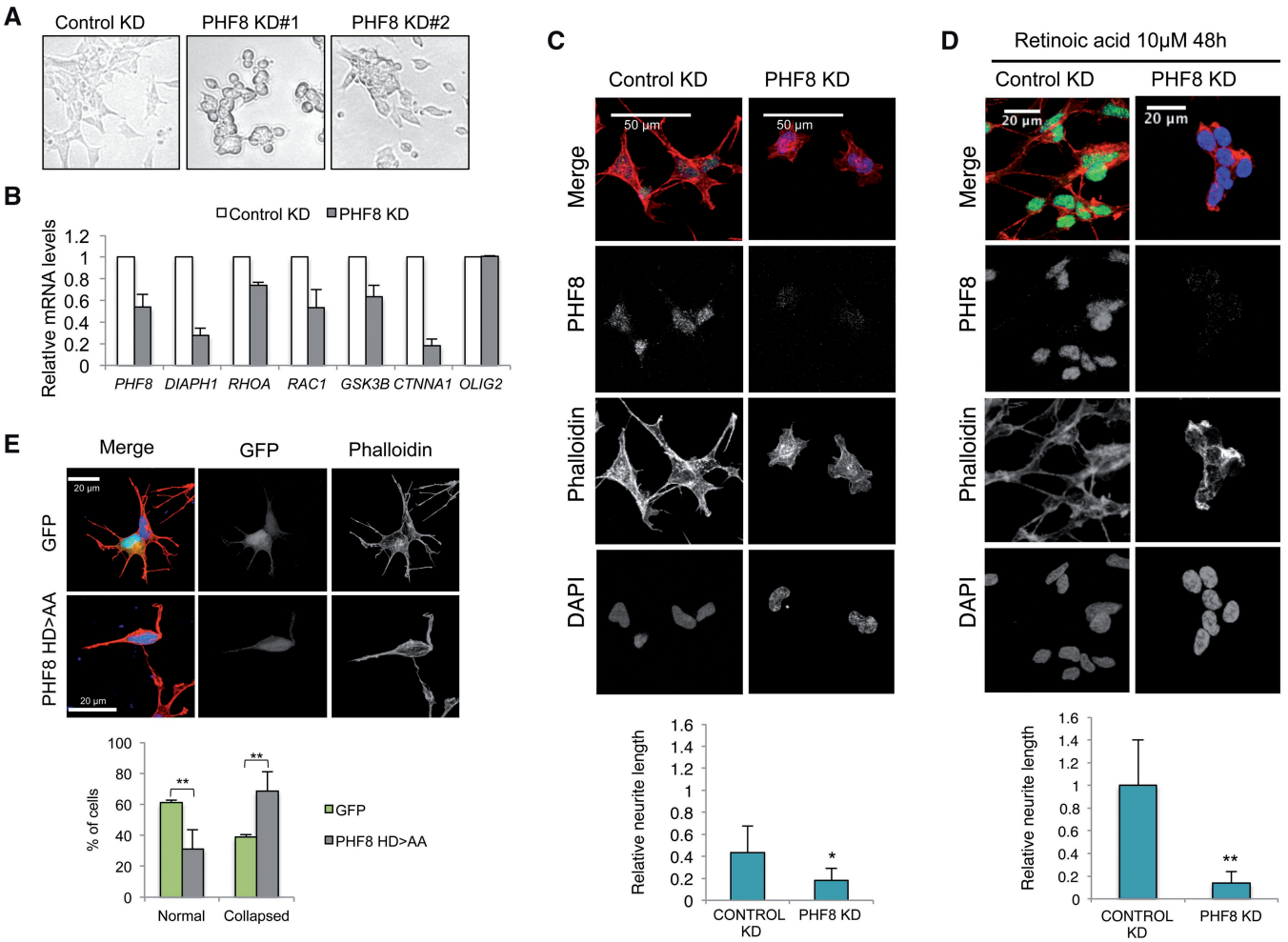

Figure 5. PHF8 is required for neurite elongation in SH-SY5Y cells. (**A**) Transmitted light photographs showing the morphology of SH-SY5Y cells stably transduced with lentiviral particles containing PHF8 shRNAs (PHF8 KD) or a random shRNA (Control KD). (**B**) mRNA levels of PHF8 target genes in Control and PHF8 KD SH-SY5Y cells. The data were normalized by 18S mRNA levels. Results are the mean of two independent experiments. Error bars indicate SD (**C**) Control and PHF8 KD cells stained with DAPI, phalloidin–rhodamine and anti-PHF8 antibody. Quantification of the total neurite length relative to the total number of cells, using ImageJ software. Data show mean of $n = 300$ cells. Error bars indicate SD $*P < 0.05$. (**D**) Control and PHF8 KD cells treated with retinoic acid 10 µM (RA) for 48 h stained with DAPI, phalloidin–rhodamine and anti-PHF8 antibody. Quantification of the total neurite length relative to the total number of cells after RA treatment. Data show mean of $n = 300$ cells. Error bars indicate SD $**P < 0.01$. (**E**) SH-SY5Y cells were transfected with pCIG (GFP) or pCIG-PHF8 HD>AA (PHF8 HD>AA). Then, cells were stained with phalloidin–rhodamine. Transfected cells (GFP positive) were analysed. The phenotype of GFP-positive cells was quantified by direct counting. Data show mean of $n = 100$ cells. Error bars indicate SD $**P < 0.01$.

to understand the molecular mechanisms responsible for this type of mental retardation. Our work links histone modifications, cytoskeleton structure and processes affected in this type of mental retardation. We demonstrate that PHF8, together with c-Myc, is recruited to promoters of genes involved in the maintenance of cytoskeleton structure. This is essential to facilitate neurite formation and/or maintenance in neuronal cells.

We demonstrate that PHF8 and Myc transcription factor bind to the same promoter regions of some target genes and that PHF8 binding is reduced after Myc depletion; these data suggest than Myc might be involved in the initial targeting of PHF8 to the analysed promoter. Other factors, such as ZNF711 (11) and E2F1 (15), interact with PHF8 and facilitate its targeting to the promoters. These data point to the possibility that proteins that directly bind chromatin could play a role in the recruitment of PHF8 to common promoters. On the other hand, it has previously been shown that the H3K4me3 mark is involved in the recruitment of PHF8 to promoters. Then, after the initial targeting by the interaction between transcription factors and PHF8, the association of PHF8 with the histone tail may contribute to stabilize the binding and to facilitate efficient catalytic activity.

We have been unable to detect an increase in overall H4K20me1 levels upon PHF8 down-regulation (data not shown), suggesting that the recruitment of a specific H4K20 methyltransferase is not a default mechanism in the cell types analysed. On the other hand, our results have shown that depletion of PHF8 leads to a local increase in H4K20me1 levels that correlates with an inefficient transcription. These data suggest that the

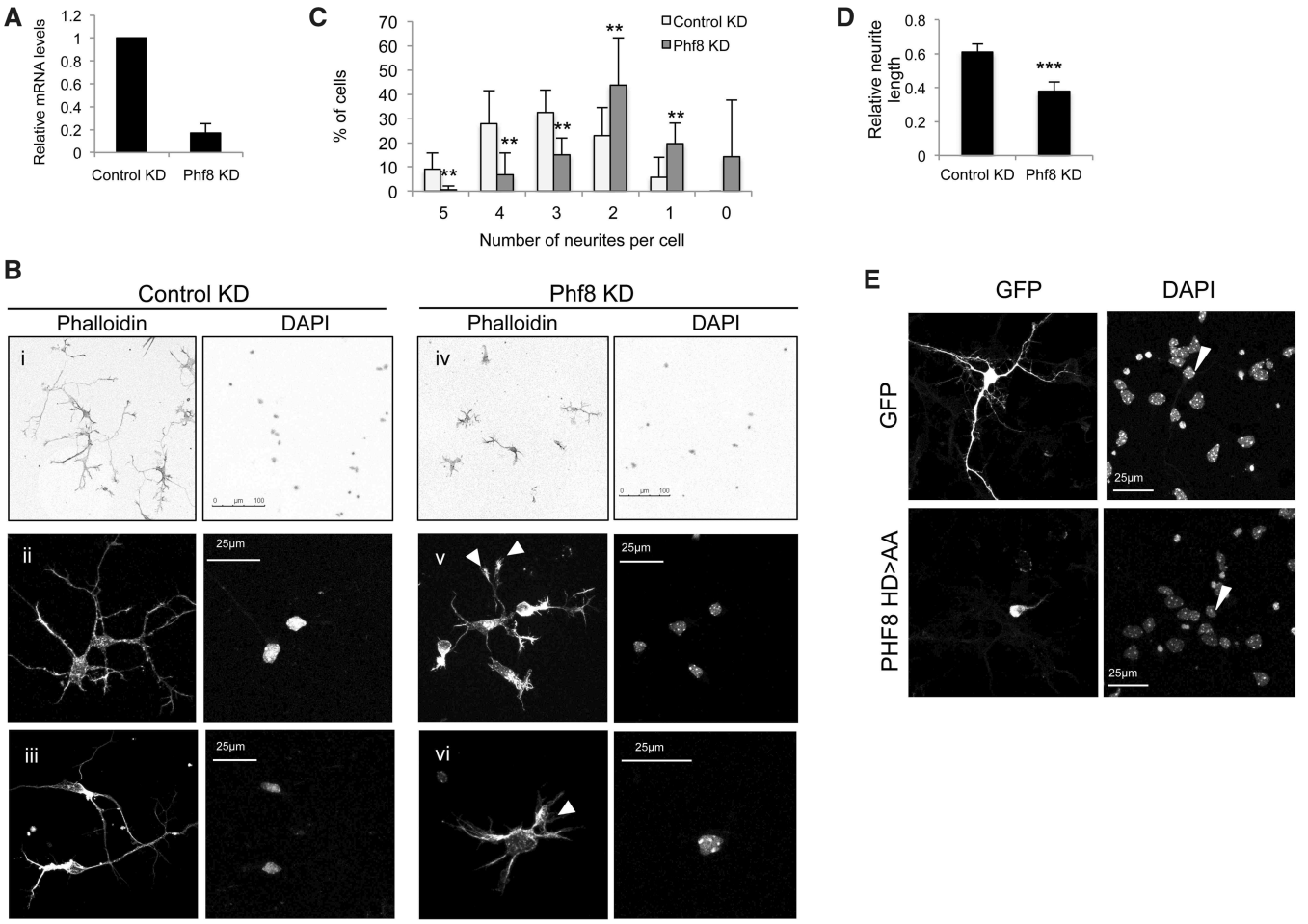

Figure 6. Cortical neurons require PHF8 for proper neurite outgrowth. (**A**) mRNA levels of mPhf8 in Control and Phf8 KD cortical neurons, normalized by Gapdh mRNA levels. Results are the mean of two independent experiments. Error bars indicate SD (**B**) Control and Phf8 KD cortical neurons stained with phalloidin–rhodamine and DAPI. (**C**) Number of dendrites per cell was quantified by direct counting of 10 randomly selected fields. Data show mean of $n = 500$ cells. Error bars indicate SD between fields. $^{**}P < 0.01$. (**D**) Neurite length of 500 cells was quantified using ImageJ software. Data show mean of $n = 500$ cells. Error bars indicate SD $^{***}P < 0.001$. (**E**) Cortical neurons cells were transfected with pCIG (GFP) or pCIG-PHF8 HD>AA (PHF8 HD>AA). Then, cells were stained with DAPI. The morphology of transfected cells was followed by GFP signal.

demethylase activity on H4K20me1 plays a role regulating transcription.

Our analyses have identified PHF8-regulated genes related to cell growth as previously described (15) and also many genes involved in cell structure and dynamics (Figure 1); namely, several components of the Rho GTPase signalling pathway (Rac1, RhoA, Diaph1), catenins (α-catenin) and its regulators (GSK3β), among others. Rho GTPases are key signalling proteins that function integrating extracellular and intracellular signals to regulate the actin cytoskeleton (33); in particular, they regulate the changes in the cytoskeleton required for neurite outgrowth and the regulation of synaptic connectivity (36,37). In line with this, mutations that alter Rho GTPase signalling result in abnormal neuronal connectivity and deficient cognitive functioning in humans (29,34). Given this, any disturbance of Rho GTPase signalling due to alterations in expression and/or regulation would have important consequences for cell physiology and function. During development, this could affect neurite outgrowth and branching as well as the guidance of axons and dendrites, leading to deficiencies in neuronal network connectivity characteristic of mental retardation (38). Moreover, in mature neurons dynamics change in neuronal cytoskeleton is also essential to respond to environmental cues. Both abilities, initial dendritic formation and dendritic plasticity, are dependent on actin cytoskeleton that is controlled by Rho GTPases (36,39,40). On the other hand, the dendritic plasticity in the mature nervous system is the basis for learning and memory functions affected in MR. However, the mechanisms responsible for the alteration of Rho GTPase activity in MR have not been completely explored.

Recently, epigenetic factors are emerged as master regulators of many key cellular functions, and then alteration of their function leads to serious pathologies. Our data show that the HDM PHF8 controls the expression levels of some essential Rho GTPase signalling components, providing a good model to study the molecular

mechanisms involved in XLMR due to low levels of Rho activity. On the other hand, understanding the molecular steps in the development of cognitive defects in MR will allow pharmacologic action with drugs to improve the cognitive function. Such a treatment could be directed to promote neurite outgrowth and normal dendritic spine number and function.

In summary, our study has revealed that PHF8 plays a key role regulating the expression of Rho GTPase signalling molecules. Accordingly, low levels of PHF8 result in deficient neurite outgrowth and stabilization. Overall, our results suggest that the mental retardation phenotype associated with loss of function of PHF8 could be due to abnormal neuron connections as a result of alterations in cytoskeleton function.

ACCESSION NUMBERS

GSE38175.

SUPPLEMENTARY DATA

Supplementary Data are available at NAR Online: Supplementary Figures 1–6 and Supplementary Methods.

ACKNOWLEDGEMENTS

We thank Dr E. Martí and Dr A. Aragay for reagents, technical help and helpful discussions. We also thank Dr X. de la Cruz for critically reviewing the paper, Dr Christoph Loenarz for the HA-PHF8 vector and Dr Keiichi Nakayama for the Flag-c-Myc vector.

FUNDING

Funding for open access charge: Spanish Ministry of Education and Science [CSD2006-00049 and BFU2009-11527 to M.A.M.B.]; Fondation Jérôme Lejeune; Fundaciò La Marató de TV3 [090210 to M.A.M.B.].

Conflict of interest statement. None declared.

REFERENCES

1. Ropers,H.H. and Hamel,B.C. (2005) X-linked mental retardation. *Nat. Rev. Genet.*, **6**, 46–57.
2. Chelly,J., Khelfaoui,M., Francis,F., Cherif,B. and Bienvenu,T. (2006) Genetics and pathophysiology of mental retardation. *Eur. J. Hum. Genet.*, **14**, 701–713.
3. Kramer,J.M. and van Bokhoven,H. (2009) Genetic and epigenetic defects in mental retardation. *Int. J. Biochem. Cell. Biol.*, **41**, 96–107.
4. Koivisto,A.M., Ala-Mello,S., Lemmela,S., Komu,H.A., Rautio,J. and Jarvela,I. (2007) Screening of mutations in the PHF8 gene and identification of a novel mutation in a Finnish family with XLMR and cleft lip/cleft palate. *Clin. Genet.*, **72**, 145–149.
5. Loenarz,C., Ge,W., Coleman,M.L., Rose,N.R., Cooper,C.D., Klose,R.J., Ratcliffe,P.J. and Schofield,C.J. (2010) PHF8, a gene associated with cleft lip/palate and mental retardation, encodes for an Nepsilon-dimethyl lysine demethylase. *Hum. Mol. Genet.*, **19**, 217–222.
6. Qiao,Y., Liu,X., Harvard,C., Hildebrand,M.J., Rajcan-Separovic,E., Holden,J.J. and Lewis,M.E. (2008) Autism-associated familial microdeletion of Xp11.22. *Clin. Genet.*, **74**, 134–144.
7. Fortschegger,K. and Shiekhattar,R. (2011) Plant homeodomain fingers form a helping hand for transcription. *Epigenetics*, **6**, 4–8.
8. Siderius,L.E., Hamel,B.C., van Bokhoven,H., de Jager,F., van den Helm,B., Kremer,H., Heineman-de Boer,J.A., Ropers,H.H. and Mariman,E.C. (1999) X-linked mental retardation associated with cleft lip/palate maps to Xp11.3-q21.3. *Am. J. Med. Genet.*, **85**, 216–220.
9. Abidi,F.E., Miano,M.G., Murray,J.C. and Schwartz,C.E. (2007) A novel mutation in the PHF8 gene is associated with X-linked mental retardation with cleft lip/cleft palate. *Clin. Genet.*, **72**, 19–22.
10. Laumonnier,F., Holbert,S., Ronce,N., Faravelli,F., Lenzner,S., Schwartz,C.E., Lespinasse,J., Van Esch,H., Lacombe,D., Goizet,C. *et al.* (2005) Mutations in PHF8 are associated with X linked mental retardation and cleft lip/cleft palate. *J. Med. Genet.*, **42**, 780–786.
11. Kleine-Kohlbrecher,D., Christensen,J., Vandamme,J., Abarrategui,I., Bak,M., Tommerup,N., Shi,X., Gozani,O., Rappsilber,J., Salcini,A.E. *et al.* (2010) A functional link between the histone demethylase PHF8 and the transcription factor ZNF711 in X-linked mental retardation. *Mol. Cell.*, **38**, 165–178.
12. Fortschegger,K., de Graaf,P., Outchkourov,N.S., van Schaik,F.M., Timmers,H.T. and Shiekhattar,R. (2010) PHF8 targets histone methylation and RNA polymerase II to activate transcription. *Mol. Cell. Biol.*, **30**, 3286–3298.
13. Tsukada,Y., Ishitani,T. and Nakayama,K.I. (2010) KDM7 is a dual demethylase for histone H3 Lys 9 and Lys 27 and functions in brain development. *Genes Dev.*, **24**, 432–437.
14. Horton,J.R., Upadhyay,A.K., Qi,H.H., Zhang,X., Shi,Y. and Cheng,X. (2010) Enzymatic and structural insights for substrate specificity of a family of jumonji histone lysine demethylases. *Nat. Struct. Mol. Biol.*, **17**, 38–43.
15. Liu,W., Tanasa,B., Tyurina,O.V., Zhou,T.Y., Gassmann,R., Liu,W.T., Ohgi,K.A., Benner,C., Garcia-Bassets,I., Aggarwal,A.K. *et al.* (2010) PHF8 mediates histone H4 lysine 20 demethylation events involved in cell cycle progression. *Nature*, **466**, 508–512.
16. Qi,H.H., Sarkissian,M., Hu,G.Q., Wang,Z., Bhattacharjee,A., Gordon,D.B., Gonzales,M., Lan,F., Ongusaha,P.P., Huarte,M. *et al.* (2010) Histone H4K20/H3K9 demethylase PHF8 regulates zebrafish brain and craniofacial development. *Nature*, **466**, 503–507.
17. Qiu,J., Shi,G., Jia,Y., Li,J., Wu,M., Dong,S. and Wong,J. (2010) The X-linked mental retardation gene PHF8 is a histone demethylase involved in neuronal differentiation. *Cell Res.*, **20**, 908–918.
18. Feng,W., Yonezawa,M., Ye,J., Jenuwein,T. and Grummt,I. (2010) PHF8 activates transcription of rRNA genes through H3K4me3 binding and H3K9me1/2 demethylation. *Nat. Struct. Mol. Biol.*, **17**, 445–450.
19. Zhu,Z., Wang,Y., Li,X., Xu,L., Wang,X., Sun,T., Dong,X., Chen,L., Mao,H., Yu,Y. *et al.* (2010) PHF8 is a histone H3K9me2 demethylase regulating rRNA synthesis. *Cell Res.*, **20**, 794–801.
20. Blanco-Garcia,N., Asensio-Juan,E., de la Cruz,X. and Martinez-Balbas,M.A. (2009) Autoacetylation regulates P/CAF nuclear localization. *J. Biol. Chem.*, **284**, 1343–1352.
21. Akizu,N., Estaras,C., Guerrero,L., Marti,E. and Martinez-Balbas,M.A. (2010) H3K27me3 regulates BMP activity in developing spinal cord. *Development*, **137**, 2915–2925.
22. Pedraza,N., Rafel,M., Navarro,I., Encinas,M., Aldea,M. and Gallego,C. (2009) Mixed lineage kinase phosphorylates transcription factor E47 and inhibits TrkB expression to link neuronal death and survival pathways. *J. Biol. Chem.*, **284**, 32980–32988.
23. Breitkreutz,B.J., Jorgensen,P., Breitkreutz,A. and Tyers,M. (2001) AFM 4.0: a toolbox for DNA microarray analysis. *Genome Biol.*, **2**, SOFTWARE0001.
24. Smyth,G.K. (2004) Linear models and empirical bayes methods for assessing differential expression in microarray experiments. *Stat. Appl. Genet. Mol. Biol.*, **3**, Article3.

25. Benjamini,Y. and Hochberg,Y. (1995) Controlling the false discovery rate: a practical and powerful approach to multiple testing. *J. Roy. Stat. Soc. Ser. B Methodol.*, **57**, 289–300.
26. Blahnik,K.R., Dou,L., O'Geen,H., McPhillips,T., Xu,X., Cao,A.R., Iyengar,S., Nicolet,C.M., Ludascher,B., Korf,I. *et al.* (2010) Sole-Search: an integrated analysis program for peak detection and functional annotation using ChIP-seq data. *Nucleic Acids Res.*, **38**, e13.
27. Valls,E., Sanchez-Molina,S. and Martinez-Balbas,M.A. (2005) Role of histone modifications in marking and activating genes through mitosis. *J. Biol. Chem.*, **280**, 42592–42600.
28. Schmidt,A. and Hall,A. (2002) The Rho exchange factor Net1 is regulated by nuclear sequestration. *J. Biol. Chem.*, **277**, 14581–14588.
29. Newey,S.E., Velamoor,V., Govek,E.E. and Van Aelst,L. (2005) Rho GTPases, dendritic structure, and mental retardation. *J. Neurobiol.*, **64**, 58–74.
30. Bellora,N., Farre,D. and Mar Alba,M. (2007) PEAKS: identification of regulatory motifs by their position in DNA sequences. *Bioinformatics*, **23**, 243–244.
31. Chan,C.H., Lee,S.W., Li,C.F., Wang,J., Yang,W.L., Wu,C.Y., Wu,J., Nakayama,K.I., Kang,H.Y., Huang,H.Y. *et al.* (2010) Deciphering the transcriptional complex critical for RhoA gene expression and cancer metastasis. *Nat. Cell. Biol.*, **12**, 457–467.
32. Guccione,E., Martinato,F., Finocchiaro,G., Luzi,L., Tizzoni,L., Dall' Olio,V., Zardo,G., Nervi,C., Bernard,L. and Amati,B. (2006) Myc-binding-site recognition in the human genome is determined by chromatin context. *Nat. Cell. Biol.*, **8**, 764–770.
33. Schmidt,A. and Hall,A. (2002) Guanine nucleotide exchange factors for Rho GTPases: turning on the switch. *Genes Dev.*, **16**, 1587–1609.
34. Ramakers,G.J. (2000) Rho proteins and the cellular mechanisms of mental retardation. *Am. J. Med. Genet.*, **94**, 367–371.
35. Nadif Kasri,N. and Van Aelst,L. (2008) Rho-linked genes and neurological disorders. *Pflugers Arch.*, **455**, 787–797.
36. Luo,L. (2000) Rho GTPases in neuronal morphogenesis. *Nat. Rev. Neurosci.*, **1**, 173–180.
37. Dickson,B.J. (2001) Rho GTPases in growth cone guidance. *Curr. Opin. Neurobiol.*, **11**, 103–110.
38. Kaufmann,W.E. and Moser,H.W. (2000) Dendritic anomalies in disorders associated with mental retardation. *Cereb. Cortex*, **10**, 981–991.
39. Chechlacz,M. and Gleeson,J.G. (2003) Is mental retardation a defect of synapse structure and function? *Pediatr. Neurol.*, **29**, 11–17.
40. Tanaka,E. and Sabry,J. (1995) Making the connection: cytoskeletal rearrangements during growth cone guidance. *Cell*, **83**, 171–176.